# EFFECT OF THERMAL COOLING CONDITIONS ON THE MICROSTRUCTURE AND HARDNESS OF MEDIUM CHROMIUM FERRITIC STAINLESS STEEL

**Amuda M.O.H.[1,2*] and Mridha, S.[2]**

[1]*Department of Metallurgical and Materials Engineering, University of Lagos, Lagos, Nigeria*
[2]*Advanced Materials and Surface Engineering Research Unit, Department of Manufacturing and Materials Engineering, International-Islamic University Malaysia, P.O. Box 10, 50728, Kuala Lumpur, Malaysia*
*E-mail: mamuda@unilag.edu.ng

## Abstract

*The characterization of the heat affected zone (HAZ) of medium chromium ferritic stainless steel (FSS) welds in terms of phases has not been exhaustive due to the dynamics of the cooling cycle from the peak temperature in the transformation range. Consequently, the relative contribution of the phases to weld property is difficult to determine. In the present work, attempt was made to approximate the HAZ of medium chromium FSS via the characterization of the effect of thermal cooling conditions on the microstructure of medium chromium FSS base metal. Two thermal cooling scenarios from four transformation temperatures-500; 800; 900; and 1100°C- were considered; and the resulting microstructure characterized using light optical microscopy (LOM), X-ray diffraction (XRD) and microhardness evaluation was compared with the HAZ of a weld of the same metal. The characterization indicated that the transformation temperature determines the types and distribution of phases present in the microstructure of medium chromium FSS. In comparison to fusion welded FSS of the same grade, the low temperature heat affected zone (LTHAZ) was approximated in the annealing temperature of 500°C while that of the high temperature heat affected zone (HTHAZ) was identified as 1100°C.*

***Keywords***: *Thermal treatment, transformation temperature, heat affected zone, phases, ferritic stainless steel*

## INTRODUCTION

Medium chromium FSS are Fe-C-Cr steels of between 16-18wt percent chromium with very low or without nickel content and having a body centred crystal structure at all temperatures (Reddy and Meshram, 2006). These steels are available under varied proprietary names. A common example of this grade of steel is the AISI 430, alternatively designated as X8Cr17, SS2320, or SUS430 depending on the designation standard adopted. Basically, they are used as general purpose material for their resistance to corrosion and scaling attack; and found application in such areas as heat exchangers, automotive exhaust

system, process equipment, vending machine and architectural trims (Shanmugan et al., 2009). These materials are usually fabricated into integrated structural unit using fusion welding. The process applies intense localized heat to join the mating surfaces. The interaction of the applied heat source with the workpiece results in reduced strength in the weld section due to the various metallurgical transformations that occur in the section (Amuda and Mridha, 2010). For medium chromium FSS, this reduction is quite high due to grain coarsening in the welds particularly in the HTHAZ. Lippold and Kotecki (2005) reported that in some of these steels the retention of the deleterious high temperature ä-ferrite in the room temperature microstructure is equally responsible for their lower mechanical properties.

The HAZ of a typical weld has various regions heated to different peak temperatures and as such exhibit complex microstructures (e.g., grain growth zone, spherodized carbide zone, etc). These complex structural identities most often possess different mechanical properties. Consequently, it has been quite difficult to approximate the properties of the HAZ (Easterling, 1992). Beside this, it has equally been difficult characterising the microstructural identities of the fusion zone. But it appears a consideration of the ternary constitution diagram for Fe-C-Cr may suffice in this instance (Lippold and Kotecki, 2005). A typical Fe-C-Cr ternary diagram for medium chromium FSS containing about 0.1 percent carbon is shown in Fig. 1. A consideration of the figure indicate that just below the solidus line ($A_4$), the microstructure consist of single phase ä which transforms to ä + ã dual phase at temperatures between 1300°C and 1100°C. However, at a temperature in the range 800°C - 1100°C, chromium carbide is precipitated from the supersaturated high temperature ä -ferrite as shown in Fig 1. Below 800°C, there is a further transformation of ä + ã dual phase to low temperature á-ferrite and carbides (Amuda, 2011). It must however be pointed out that the scenario just described is for equilibrium condition which is not applicable to fusion welding due to the dynamics of the rapid heating and cooling associated with fusion welding. Therefore, it is expected that there would be a variation in the microstructure of the HAZ relative to the Fe-Cr pseudo constitutional diagram; and this indeed is the case (Lippold and Kotecki, 2005).

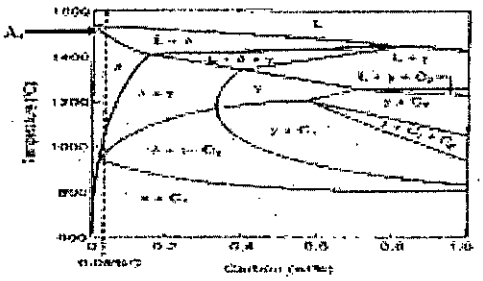

Fig.1 Constitution diagram for medium chromium Fe-C-Cr pseudo binary diagram (Lippold and Kotecki, 2005)

While the peak temperature is very important in determining the degree of re-austenitization in different portions of the HAZ during the heating cycle, the cooling rate is more important in the development of

microstructure during cooling, and this is best illustrated in Fig. 2 using a continuous cooling transformation (CCT) diagram of a material that has been rapidly heated to a temperature close to the melting point where ä-ferrite is stable (Pistorious and Van Rooyen, 1995). Cooling rates higher than the rate *aa* results in a fully ferritic HTHAZ, on the other hand, cooling rate lower than *bb* produces a completely martensitic structure. For cooling rates in between these two extremes, the HTHAZ consists of a duplex martensite and ferrite structure. Further cooling of the duplex structure may result in partial transformation of ä-ferrite to ã which ultimately transform to martensite. This invariably suggests that the cooling rate from the various peak temperatures in the different regions of the HAZ determines the phases present in the microstructure.

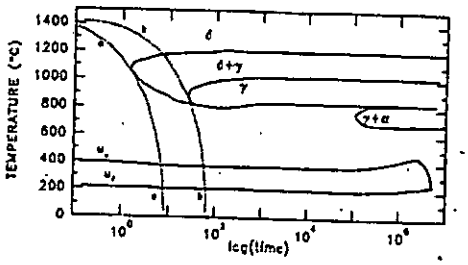


Fig.2 Continuous cooling transformation of ä-ferrite to ã in the HTHAZ during weld thermal cycle (Pistorious and Van Rooyen, 1995)

During annealing treatment, a number of metallurgical reactions can occur depending on the annealing temperature. Some of the possible reactions include formation of a new phase, dissolution of secondary phase, recrystallization and grain refining. For instance, during the heating cycle of thermal treatment, any carbide and other precipitates will likely dissolve; martensite will equally tend to dissolve by reverting to ferrite accompanied by carbide formation or transforming back to austenite. The metallurgical reaction occurring during conventional thermal treatment has been approximated and extended to the treatment of the HAZ region of welds and as such, the CCT curve is often used to describe solid state transformation behaviour in welds (Easterling, 1992). However, as represented by Figs 3(a) and 3(b) respectively, the thermal cycle in a conventional thermal treatment is quite distinct from that of weld thermal cycle. Fig. 3a is a typical thermal treatment profile while Fig.3b shows the profile from welding process. Thermal treatments involve a soak time at a specified temperature, usually around the $Ac_3$ (910°C) temperature, followed by a constant cooling period. Fig. 3b shows that the peak temperature during welding varies with distance from the weld centreline, and the accompanying cooling rate is not constant. The figures indicate that the peak temperatures reached in the HAZ can be very much higher than the $Ac_3$. The heating rates are quite high, and the time spend at high temperatures is only of the order of a few seconds. This produces a very steep temperature gradient and complicates the attempts at studying the in-situ transformations in the HAZ during welding. In order to ascertain the effect of a weld thermal cycle on a particular FSS, it is not possible to use methods that may be applicable to other heat treatments.

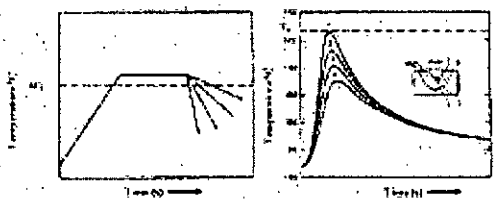

(a) (b)

Fig.3 Thermal cycle comparison between heat treatment and welding; (a) thermal cycles from conventional annealing treatment and (b) typical weld thermal cycles (Ravi Vishnu, 1995)

CCT diagrams such as the one presented in Fig.2 often gives an approximate idea of the transformation behaviour in the HAZ of welds. It has been used to predict quite reasonably the metallurgical features of the zone (Pistorious and Van Rooyen, 1995) and the diagram is invoked to characterize the microstructure of medium chromium FSS using conventional thermal treatment.
In the HAZ, four different regions have been identified that approximate different peak temperatures (Easterling, 1992); and these are the coarse grained region (e"1100°C), the grain refined region (H"900°C), the intercritical region (H"800°C) and the subcriticical region (H"500°C). In spite of these delineations, the characterization of the HAZ of medium chromium FSS welds in terms of phases has not been exhaustive due to the dynamics of the cooling cycle from the weld peak temperature in the transformation range. As a result, the relative contribution of the phases to weld property is difficult to determine. Therefore, in the present paper, the effect of thermal cooling conditions on the microstructure and hardness of medium chromium FSS base metal is investigated. Two thermal cooling scenarios from four transformation temperatures-1100; 900; 800; and 500°C-were considered; and the resulting microstructure characterized using LOM, XRD and microhardness evaluation was compared with the HAZ of a weld of the same metal. This present investigation is expected to provide understanding into the predominant cooling dynamics during the downhill cycle of fusion welding process.

## Materials and Method

The medium chromium FSS conforming to AISI 430 used in this investigation was supplied by Cenco Sains, Malaysia in the cold rolled condition having the chemical composition listed in Table 1. The 1.5 mm thick FSS was prepared into 65 mm x 25 mm dimension and pre-cleaned in acetone using Branson 2510 ultrasonic cleaner at solution temperature of 30°C for 10 minutes.

Table1: Chemical composition of AISI 430 FSS provided by the supplier and complemented with EDXRF spectroscopy

| Material Spec. | Composition | | | | | | | KFF | $Cr_{eq}$/ $Ni_{eq}$ |
|---|---|---|---|---|---|---|---|---|---|
| AISI | C | Cr | Ni | Si | Mn | P | S | 14.7 | 3.85 |
| 430 | 0.12 | 16.19 | - | 0.75 | 1.0 | 0.04 | 0.30 | | |

Sixteen pre-cleaned samples were encased in quartz filled steel tube and subsequently solution annealed at four different temperatures of 500, 800, 900 and 1100°C, respectively in muffle laboratory furnaces with maximum thermal capacity of 1500°C. The quartz encasement was to prevent the oxidation of the samples in the oxidizing environment of the annealing furnace. The material and facility set-up for the experiment is presented in Fig. 4. The investigation adopted equal heating rate of 17°C/min for the different annealing temperatures, though the time to the different temperatures varies. The samples were soaked at these temperatures for 60 and 120 minutes respectively; and subsequently cooled in two different media. A group of four samples was normalized while another group of four was water quenched. The thermal treatment conditions of the investigation are provided in Table 2.

The samples were sectioned, ground and polished mechanically using different grits of silicon carbide paper and 0.5 micron deagglomerated alpha alumina; and subsequently prepared for microstructural examination by etching in a solution of 15 ml HCl, 10 ml acetic acid, 5 ml $HNO_3$ and 2 drops of glycerol.

Microstructural examination was effected with a Nikon Epiphot 200 inverted optical microscope with image analysis software. Microhardness measurement was taken on freshly polished samples using Mitutoyo microhardness tester at a test load of 0.5 kgf for a dwell time of 10s.

Laboratory muffle furnace rated 1500°C
Ceramic support to prevent adhesion of steel tube to the furnace hearth
Steel tube housing the quartz encasement
Sample encased in quartz

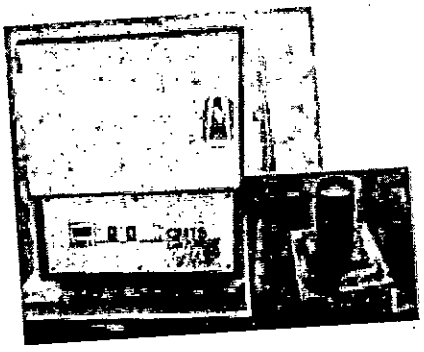

Fig. 4 Illustration of the set-up for the thermal treatment experiment

XRD study of the samples was carried out to qualitatively characterize the phases present in the differently thermally cooled samples. The study utilized Shimadzu 600 X-ray diffractometer with a diffracted beam monochromator using CuKá radiation maintained at 2 Kw, 40 Kv and a current of 30 mA as the excitation source.

| Annealing Temp. (°C | Soaking Time (min) | | Cooling Sequence |
|---|---|---|---|
| | Heat 1 | Heat 2 | |
| 500 | 60 | 120 | Normalizing/ water quenching |
| 800 | | | |
| 900 | | | |
| 1100 | | | |

**Table 2: Thermal treatment conditions**

## RESULTS AND DISCUSSION

The initial microstructure of the as-received medium chromium FSS sample in Fig. 5a contains ferrite surrounded by carbides aligned in the rolling direction. Fig. 5b is the representative microstructure of HAZ of welds of the sample for comparison with the thermal treatment cycle. In medium chromium FSS, martensite formation in welds is inevitable once the KFF is less than 17 (Kaltenhauser, 1971). Similarly, the $Cr_{eq}$/ $Ni_{eq}$ must be greater than 5 to avoid the formation of martensite in the weld microstructure (Folkhard, 1988; Amuda, 2011). These values predict the tendency for martensite to form in the weld section of alloys (Lippold and Kotecki, 2005). In the present investigation, the KFF and $Cr_{eq}/Ni_{eq}$ values listed in Table 2 suggest that martensite will form in the weld section of the alloy and this is indicated in Fig.5b as a continuous network at the grain boundary of the ferrite matrix. The figure equally show the presence of coarse ferrite grains surrounded by continuous networks of martensite formed from the elevated temperature austenite. The existence of intragranular precipitates is indicated by the presence of peppery carbides ($Cr_{23}C_6$) within the matrix of the ferrite.

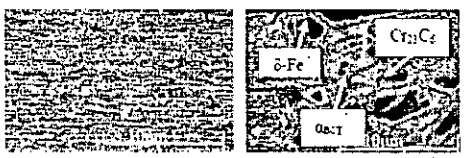


Fig.5 Microstructure of AISI 430 FSS (a) as-received; (b) HAZ section of its weld

Figs. 6 and 7 are the microstructures of samples annealed at different temperatures for 60 minutes but normalized in air and quenched in water respectively. The microstructure of the sample annealed at 500°C (Fig. 6a) show the presence of room temperature á-ferrite and grain boundary carbide precipitates, essentially as the as-received sample except that the grains are more refined and the deformation effect has been removed. The Fe-Cr-C constitution diagram (Fig. 1) indicates that at 500°C, the sample is still below the lower critical temperature ($AC_1$) and at this level no polymorphic transformation can occur; however, there is slight grain refinement and this is represented in the equiaxed structure of the matrix. Comparing Fig. 6a with Fig 5b suggest that the LTHAZ of welds can be approximated by Fig. 6a. Annealing at 500°C probably has a tempering and refining effect. Fig.6b is not quite different from Fig. 6a except that there is appreciable reduction in the carbide precipitate indicating that as the annealing temperature increases, there is increase in dissolution of the second phase precipitates. This is in agreement with the Fe-Cr-C constitution diagram. At 900°C (Fig. 6c), austenite transformation occurs taking carbon into solution, the precipitate therefore dissolves. However, austenite being an effective grain growth inhibitor prevents accelerated grain growth in the ferrite matrix, and this enhances the formation of equiaxed grains in the microstructure. More also, the soaking time of 60 minutes also restricts diffusion from the adjacent matrix and ensures grain stability. This temperature

probably corresponds to grain recrystallization temperature. The sample solution annealed at 1100°C (Fig. 6d) is in the two phase (ä + ã) field and during slow cooling, the solubility of carbon in the high temperature ä-ferrite reduces and this is precipitated as carbides within the grains of the ä-ferrite thus generating intragranular precipitation with the stable austenite at the grain boundaries. Below 900°C, the austenite transforms to á-ferrite and carbide. The á ferrite is also supersaturated in carbon; the excess carbon in the ferrite is subsequently precipitated as carbides at grain boundary. it is implied therefore that the 1100°C treated sample after normalizing consist of intragranular carbides in ferrite matrix surrounded by grain boundary carbides arising from the precipitation of excess carbon from supersaturated á-ferrite solid solution but without martensite (Lippold and Kotecki, 2005). This is shown in - Fig. 6d.

Fig.6 microstructures of samples annealed at different temperatures and normalized in air:
(a) 500°C, (b) 800°C, (c) 900°C and (d) 1100°C

Fig.7 presents the microstructure of the sample solution annealed at the same conditions as Fig.6 but quenched in water. Figs. 7a and b are not appreciably different from Figs.6a and b. This is expected because the treatment temperature is below the transformation temperature that could have caused dissolution of the second phase carbide precipitates. The only noticeable difference is that the quenched samples appear to have better refined grains relative to the normalized samples. Fig.7c show the microstructure produced by quenching in water at 900°C. The microstructure consists of martensite along the high temperature ä-ferrite grain boundaries with sparse presence of intragranular carbides. The very low presence of intragranular carbides is due to the partitioning and dissolution of the original carbides from ferrite into austenite during the heating cycle owing to the higher solubility of carbon in austenite. Quenching from this temperature prevents the dissolved carbon from precipitating out; and as such, it is retained in the martensite while the undissolved carbides are precipitated as sparse intragranular types of carbide (Lippold and Kotecki, 2005; Folkhard, 1988).

Fig.7 microstructures of samples annealed at different temperatures and quenched in water at ambient condition: (a) 500°C, (b) 800°C, (c) 900°C and (d) 1100°C

The microstructure of the sample annealed at 1100°C but quenched in water shown in Fig. 7d consists of martensite plates along the ferrite boundaries and intragranular precipitates. The intragranular precipitates develop because, consequent upon quenching, diffusion is inhibited resulting in the supersaturation of the room temperature á-ferrite. The excess locked up carbon in the supersaturated phase is ultimately

precipitated within the grain interior as intragranular carbides.

Figs. 8 and 9 are the micrographs of samples annealed at different temperatures for 120 minutes; normalized and quenched in water respectively. Fig. 8a show bigger carbide grains due to increase soaking time which improves the diffusion of adjacent carbide grains. This results to coalescence of adjacent grains and coarsening of the carbides. This trend is also visible in Fig. 8b but with a higher level of grain coarsening due to the composite influence of increased annealing temperature and soaking time. Annealing at 900°C followed by normalizing show that there is enhanced dissolution of carbide in the austenite phase in a predominantly ferrite matrix (Fig.8c). The microstructure at this instance show increased dissolution of the carbides in the two phase region due to enhanced soaking time at the elevated temperature. The room temperature microstructures show a ferrite matrix with intergranular precipitates rather than intragranular obtained when the sample was annealed at 900°C for 60 minutes. Fig. 8d is not quite different from Fig.8c except that the grains are apparently bigger with less distribution of the precipitates. This indicates that the dissolution of the carbides into the austenite is greater at this level; and that the treatment temperature and soaking time permits diffusion of the adjacent grains leading to coalescence of the grains.

Fig.8 microstructures of samples annealed at different temperatures for 120 minutes and normalized in air: (a) 500°C, (b) 800°C, (c) 900°C and (d) 1100°C

Figs. 9a and 9b present similar microstructural features to Figs. 8a and b except that the grains are a bit refined due to the fast cooling from the annealing temperature. The fast cooling inhibits diffusion process and as such grain coalescence is prevented resulting in some sort of grain refinement. Figs.9c and d show the presence of martensite along the ferrite grain boundaries and intergranular carbide for samples soaked for two hours at 900°C and 1100°C respectively and quenched in water. However, the grains of the 1100°C quenched samples appears larger due to the higher annealing temperature coupled with the soaking time of 120 minutes. This permits the diffusion of adjacent grains resulting in the coalescence of the grains (Folkhard, 1988).

Fig.9 Microstructures of samples annealed at different temperatures for 120 minutes and quenched in water at ambient condition: (a) 500°C, (b) 800°C, (c) 900°C and (d) 1100°C

Fig. 10 shows the microhardness chart for the samples at different test conditions with standard deviation between 1.89 and 11.34 for all the conditions investigated. This is generally within the allowable limits. However, the very high standard deviation of 11.34 statistically recorded in samples austenitized at annealing temperature of 1100°C suggests the presence of phases

other than equilibrium phases. It is most probable that retained austenite is present in the microstructure under this condition. The figure equally show that for a given annealing temperature, the water quenched sample at soaking time of 60 minutes gives the highest microhardness value. This is expected because fast cooling inhibits diffusion and hence prevents grain coalescence and coarsening (Barlow, 2009). It is evident from the chart

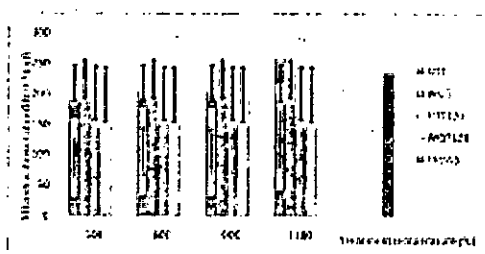

Fig.10 Microhardness chart for the differently thermally cooled samples and the control weld sample (NTT=normalized treatment, WQT=water quenched, FSSWS=control weld sample)

that the hardness increases with increasing annealing temperature irrespective of the cooling sequence particularly at annealing temperatures of 900°C and 1100°C. This trend is probably due to increase in the dissolution of the carbide into austenite at higher temperatures with increased carbon solubility. In comparison, the microhardness value of the controlled weld sample in Fig.10 show that the character of the sample is approximated by the annealing temperatures between 900°C and 1100°C. This suggests that the HTHAZ is approximated by the thermal conditions between 900°C and 1100°C.

The dissolution of carbides into austenite at the dual phase region at these temperatures prevents grain growth and subsequent quenching from these temperatures retains the supersaturated condition. In this state, the samples are hardened with the presence of both intragranular and intergranular precipitates. The microhardness value is consequently high. However, soaking for 120 minutes increases the diffusion of adjacent grains and coalescence of grains results. This creates larger grains with attendant loss in hardness values. This explains the basis for the low hardness value obtained in the 120 minutes soaked samples relative to those soaked for 60 minutes. But, comparing the thermal cycle during thermal treatment with that during welding as indicated in Fig.3 show that heating rate during welding is very rapid unlike in conventional thermal treatment and that the time spend above the peak temperature in welding is very transient likewise the cooling cycle. Therefore, the 120 minutes soaking time is never approximated in real-time welding not even in multi-pass welds. This condition deserves no further consideration in the present discussion and is subsequently discontinued in the XRD characterization. Of particular significance is the fact that different positions in the HAZ of welds are heated to different peak temperatures. Therefore, it might not be appropriate to use the thermal cycle conditions during conventional thermal treatment to characterize weld thermal cycle since the dynamics of the two processes is different.

However, the present study has shown that it might be possible to approximate the thermal condition during welding at the LTHAZ with the conventional quenching from 800°C and/or 500°C in water at ambient condition. Consequently, the LTHAZ of Fig.5b can be approximated by the microstructures of Figs. 7a and b.

Figs. 11 and 12 are the XRD spectra for samples annealed for 60 minutes and afterwards normalized and quenched in water respectively. Fig.11 show that at 500°C, the phases present after normalizing are á-Fe and chromium carbide of the type $Cr_{23}C_6$ corresponding to the diffraction plane (110)/(200) and (222) for á-Fe and $Cr_{23}C_6$ respectively. It appears that the carbide present at this condition is rather sparse. However, in the temperature range 800-1100°C, there are additional peaks corresponding to $Cr_{23}C_6$ along with the matrix. The additional peaks seem to increase with the annealing temperature. This suggests that more chromium carbide is precipitated in the matrix and this apparently explain the increase in the microhardness value observed in Fig.10 across the annealing temperatures.

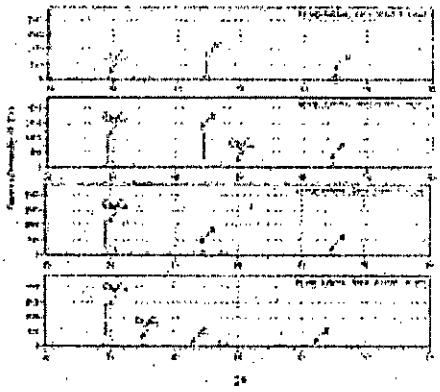

Fig.11 XRD pattern for normalized samples

The spectra of Fig. 12 particularly at about 29° diffraction angle for annealing temperatures 800-1100°C show stronger peaks than those obtained at 500°C. These higher peaks are considered to be intragranular carbides that could not be precipitated due to the inhibition of diffusion by the quenching process. The peaks at about 65° diffraction angle are believed to be martensite. There are also some weak chromium carbide peaks suggesting the presence of very low intragranular chromium carbides.

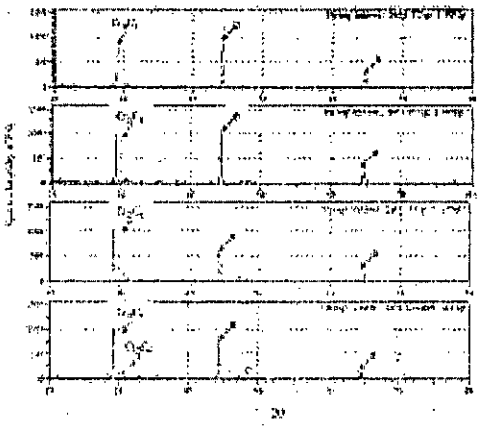

Fig 12 XRD pattern for quenched sample

## CONCLUSION

Medium chromium FSS subjected to normalizing and quenching treatments at different annealing temperatures and soaking time have been characterized using LOM, XRD and microhardness evaluation and compared with the HAZ of a weld of the same metal.

The following facts emerged from the study:

i. The cooling dynamics of weld section is quite different from conventional thermal treatment and can hardly be approximated by the continuous cooling curve.

ii. The LTHAZ can be approximated by the thermal conditions during quenching from 500°C while the HTHAZ is approximated by quenching from 1100°C.

iii. The XRD spectral show the presence of both intergranular and intragranular carbides whose pattern corresponds to diffraction pattern for $Cr_{23}C_6$ in normalized samples and the presence of martensite in quenched sample.


## ACKNOWLEDGEMENTS

The authors acknowledge the International Islamic University Malaysia for granting a visiting research position to the lead author for the preliminary work documented in this paper.


## REFERENCES


Amuda, M.O.H. (2011). Microstructures and properties of TIG melted AISI 430 ferritic stainless steel welds. Doctoral thesis. International Islamic University Malaysia, Kuala Lumpur.

Amuda, M.O.H. and Mridha, S. (2010). Grain refinement in ferritic stainless steel, the journey so far. *Adv. Mat. Res.* **83-86**: 1165-1172.

Barlow, L.D. (2009). The effect of austenitizing and tempering parameters on the microstructure and hardness of martensitic stainless steel AISI 420. M.Sc. dissertation. University of Pretoria, Pretoria.

Easterling, K. E. (1992). Introduction to physical metallurgy of welding. 2nd edn. Butterworth-Heinemann, Oxford.

Folkhard, E. (1988). Welding metallurgy of stainless steel, New York, Springer-Verlay.

Kaltenhauser, R.H. (1971). Improving the engineering properties of ferritic stainless steel. *Metal Eng. Q.* **11 (2)**: 41-47.

Lippold, J. C. and Kotecki, D. J. (2005). Welding Metallurgy and Weldability of Stainless steel. Wiley-Interscience, New York.

Pistorious, P.G.H. and Van Rooyen, G.T. (1995). Composition and properties of ferritic stainless steels with good weldability. *Weld. in the World.* **36**: 65-72.

Ravi Vishnu, R. (1995). Solid-state transformations in weldments. ASM Metals Handbook, *Volume 6: Welding, Brazing and Soldering*. ASM Materials Park, Ohio, pp 70-71.

Reddy, G. M. and Meshram, S.D. (2006). Grain refinement in ferritic stainless steel welds through magnetic arc oscillation and its effect on tensile property. *Indian Weld. J.* **42**:35-41.

Shanmugan, K., Lakshminarayanan, A. and Balasubramanian, V. (2009). Effect of weld metal properties on fatigue crack growth behaviour of gas tungsten arc welded AISI 409M grade ferritic stainless steel joints. *Int. J. Press. Vessels and Piping*. **86**:517-524.